

**Nonlinear fluorescence spectroscopy of layered perovskite quantum wells**

**Ran Gao**

Under the Direction of Prof. Andrew M. Moran

Department of Chemistry  
The University of North Carolina at Chapel Hill

3/15/2022

## 1. Introduction:

Renewed interest in layered hybrid perovskite quantum wells is motivated by optoelectronic applications including photovoltaic devices<sup>1-4</sup>, light-emitting diodes<sup>5</sup>, and microcavity lasers<sup>6</sup>. In these systems, quantum wells with a range of thicknesses are distributed such that the average values of the bandgaps and energy levels vary monotonically with respect to depth in the films<sup>7-9</sup>. Charges and energy can transfer between quantum wells with different levels, which is closely related to energy efficiency of the optical devices that include perovskites. As a result, scientists are developing new spectroscopy techniques to study the dynamics of charged particles in perovskite layers. To be specific, to improve the energy transfer efficiency, scientists need to know the time that the charged particles take to travel between different quantum wells. Nonlinear fluorescence spectroscopy developed by our group is a sensitive technique that can be applied to study this theme.

A common layered perovskite material has a structure formula of  $(BA)_2(MA)_{n-1}[Pb_nI_{3n+1}]$ , where MA is methylammonium and BA is n-butyl ammonium. The crystal structure of perovskite is shown below:

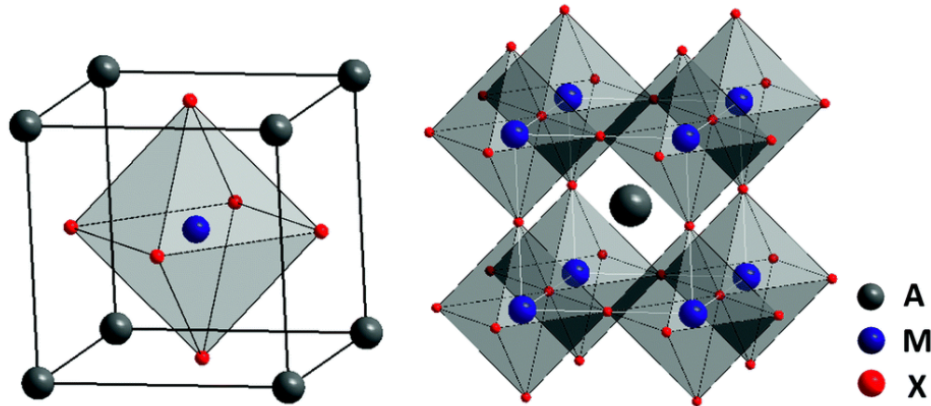


**Figure 1.** Structure of perovskite material. *A* is an organic cation such as methylammonium. *M* is a metal ion such as lead. *X* is a halogen atom such as iodine.

In this paper, I focused on two-dimensional perovskite films, for the recent work has shown that quantum-confined 2D perovskites show long-term stability while maintaining solar cell efficiencies on the order of 18%<sup>10</sup>. A 2D layered perovskite material is shown below:

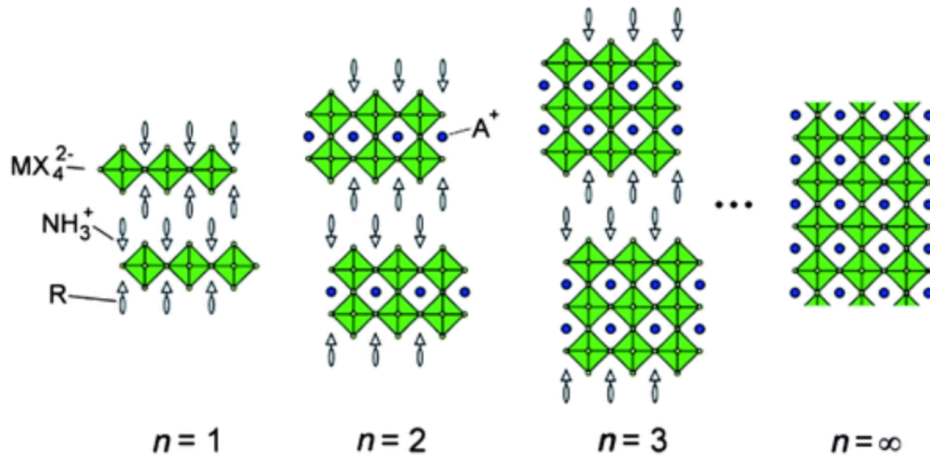


**Figure 2.** The structure of 2D perovskite where  $A$  is an organic cation such as methylammonium,  $M$  is a metal ion such as lead, and  $X$  is a halogen atom such as iodine, bromine, or chlorine.  $(BA)_2(MA)_{n-1}[Pb_nI_{3n+1}]$  is one of the 2D perovskite formulas, where  $MA$  is methylammonium and  $BA$  is  $n$ -butyl ammonium. The index,  $n$ , governs the thicknesses of a quantum wells which is in turn reflected in the resonance wavelengths of excitons.

In 2D perovskite systems, there are different quantum wells with different number of layers of perovskite lattice. When the light is applied to the quantum wells, electrons in the valence band will be excited into the conduction band, forming a hole in the valence band. The excited electron and the hole can associate with each, forming a pair known as an exciton. When the excited electron recombines with the hole, the system returns to the ground state again. Photoexcited excitons are quantum-confined in 2D perovskites because the energy gap of perovskite layers is much narrower than the energy gap of the organic layers. In this case, perovskite layer forms a potential well while the organic layers have a much higher potential energy, which confine the excitons within the perovskite quantum wells.

Quantum wells with different energy levels have different energy gaps, leading to different absorption resonance. In other words, quantum wells absorb lights at different wavelengths. For example, in layered perovskite system with  $n$ -butyl ammonium spacer,  $n=3$  quantum wells have the largest light absorption at 600 nm while  $n=4$  quantum wells have the largest light absorption at 645 nm.  $N=5$  quantum wells even have a larger absorption at 680 nm. Larger quantum wells absorb redder light. When distributing on a film, smaller quantum wells are more concentrated on the glass side while the large quantum wells are concentrated on the air side, which is shown in **Figure 3**. The films are configured in this way to promote energy and electrons to transfer from smaller quantum wells to bigger quantum wells, forming an energy funnel as shown in **Figure 4**. This is because energy gap decreases as the index of the quantum well,  $n$ , increases. This can be visualized similar to the particle-in-box model. The energy gap decreases as the size of the box increases. Similarly, the energy gap decreases as the size of quantum well increases. As a result, excitons in larger quantum wells have lower energy than those in smaller quantum wells do, leading to a tendency of energy transport towards quantum wells.

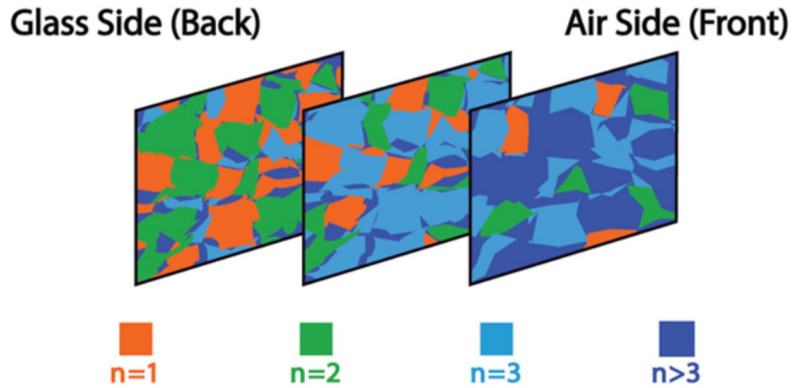


**Figure 3.** Concentrations of organohalide perovskite quantum wells exhibit a layering effect in the targeted systems. The smallest and largest quantum wells are most concentrated near the glass and air interfaces of the film, respectively.

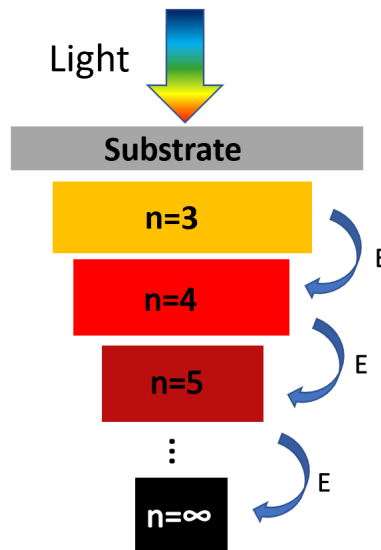


**Figure 4.** This is a scheme of energy funnel in perovskite quantum wells. The energy will transfer from small quantum wells to big quantum wells simultaneously.

Applied to study the photo-induced relaxation mechanisms of 2D layered perovskite, conventional transient absorption (TA) experiments show that the energy transfer process between quantum wells happens on sub-ns time scale and is facilitated by the large exciton transition<sup>13</sup>. As shown in **Figure 5**, in TA spectroscopy, we first apply a pump light to small quantum well, which is n=3 quantum well for example. The pump light excites the electrons in n=3 quantum well and form excitons there, indicating the initial position of excitons. Then a probe light is applied to a bigger quantum well, which is n=4 quantum well for example. The probe light tells the current position of excitons, which means excitons are in n=4 quantum wells now. A TA signal is collected from there, with the information that excitons were in n=3 quantum wells initially and now exist in n=4 quantum wells, indicating that energy was transferred from n=3 quantum wells into n=4 quantum wells. However, TA technique has a

shortage that we miss the information of the exciton position after it reaches  $n=4$  quantum well. In other words, we don't know what happens to excitons after the TA signal is collected from  $n=4$  quantum well. We want to figure out whether the excitons keep traveling to bigger quantum wells or they in  $n=4$  quantum wells without further movement.

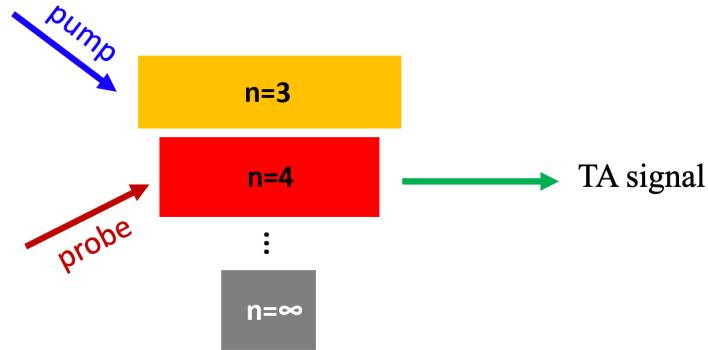


**Figure 5.** Technical scheme of TA spectroscopy. A pump is applied to  $n=3$  quantum wells, indicating the initial position of excitons. Then a probe is applied to  $n=4$  quantum wells, indicating the current position of excitons. A TA signal is then collected from there.

In this case, coherent two-dimensional (2D) fluorescence spectroscopies, in which the nonlinear response is isolated by a sequence of four laser pulses, have been demonstrated in recent years as a solution. Higher sensitivity has been reached by this new technique because of its background-free nature. Moreover, it has a potential to offer us a new degree of freedom by dispersing the emission to an array detector. These advantages of fluorescence detected spectroscopies can benefit the research on layered perovskite. In this paper, I used nonlinear fluorescence (NLFL) spectroscopy that is recently developed by our group to study the relaxation mechanisms in 2D layered perovskite systems. NLFL is similar to TA by having two pulses. An example is shown in **Figure 6**. We first apply pulse 1 to  $n=3$  quantum well, forming excitons in  $n=3$  quantum well. Pulse 1 indicates the initial location of excitons. Then we apply pulse 2 to  $n=4$  quantum well, indicating the intermediate location of excitons. Finally, we measure fluorescence around 700 nm from large quantum wells, indicating the final location of excitons. The fluorescence is measured with a bandgap which collects the light between 700 nm to 725 nm. This is because large quantum wells have the largest absorption wavelength of 700 nm, and the fluorescence emission of those large quantum wells should be a little longer than the largest absorption wavelength. By keep the wavelength of pulse 1 constant at 590 nm, we can know the initial location of excitons is always  $n=3$  quantum wells. By shifting the wavelength of pulse 2 over a range from 560 nm to 680 nm, we can know the intermediate locations of excitons in different quantum wells. This is how we conduct 1D NLFL measurements.

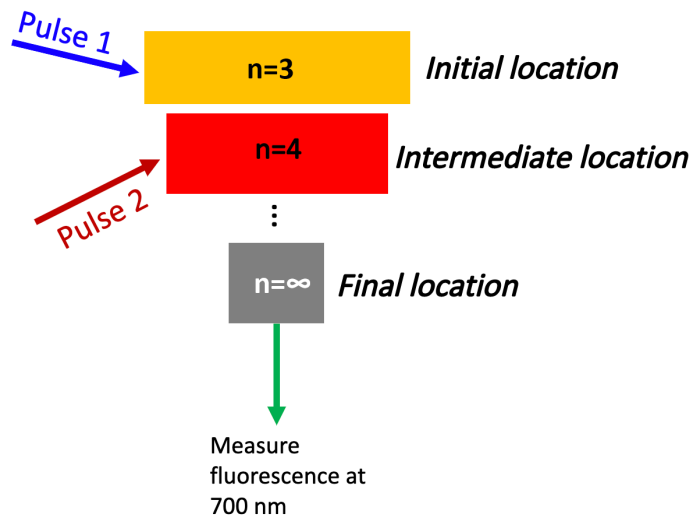
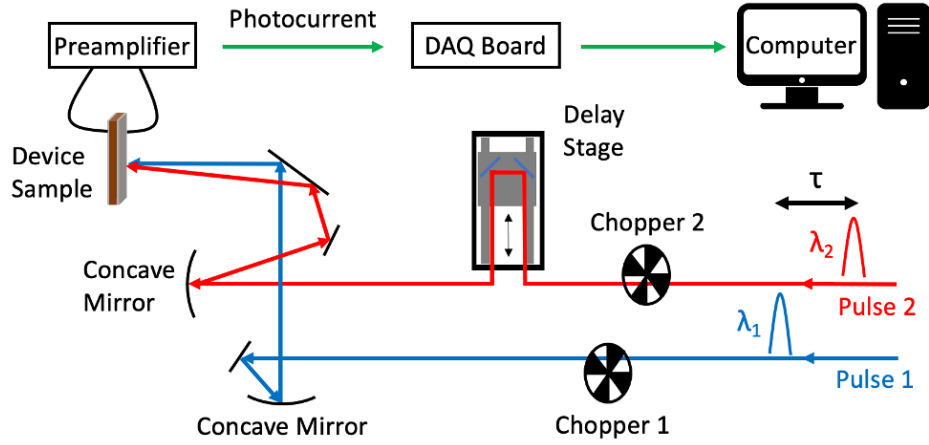


**Figure 6.** Technical scheme of NLFL spectroscopy. Pulse 1 is applied to  $n=3$  quantum well, indicating the initial position of excitons. Then pulse 2 is applied to  $n=4$  quantum well, indicating the intermediate position of excitons. Finally, fluorescence at 700 nm is measured from large quantum wells, indicating the final location of excitons.

**Figure 7** shows how NLFL signals are created. As mentioned before, the experiment is conducted with two narrowband laser beams (5 nm spectral widths) that are tunable in the visible spectral range, shown as pulse 1 and pulse 2 below. The nonlinear response of the fluorescence is isolated by chopping the beams at different frequencies as described in the experimental methods section below. The wavelength of pulse 1 is constant, while the wavelength of pulse 2 and the delay time between two pulses,  $\tau$ , are varied to produce one-dimensional NLFL spectra.

(a)



(b)

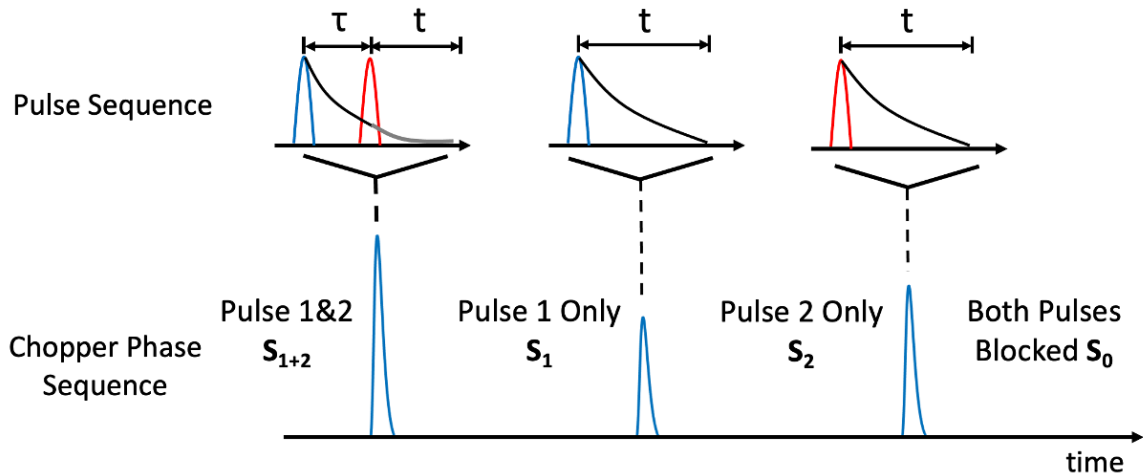


**Figure 7. (a)** Fluorescence emission induced by a pair of color-tunable laser pulses is measured in NLFL spectroscopy. The two pulses are chopped at different frequencies. Pulse 1 is chopped at 500 Hz and pulse 2 is chopped at 250 Hz. The wavelength of pulse 1 is constant, while the wavelength of pulse 2 and the delay time between two pulses,  $\tau$ , are varied to produce one-dimensional NLFL spectra. **(b)** By chopping two pulses at different frequencies, 4 phases are created. NLFL signal is collected by  $S_1$  and  $S_2$  from  $S_{1+2}$ .

## 2. Experimental Methods:

### 2.1 Fabrication of Perovskite Film

According to the structure formula of perovskite,  $(\text{BA})_2(\text{MA})_{n-1}[\text{Pb}_n\text{I}_{3n+1}]$ ,  $n=2$  and  $n=3/4$  samples are made using n-butyl ammonium, methylammonium, and lead (II) iodide. Ideally,  $n=2$  sample is supposed to contain  $n=2$  perovskite quantum well only, and  $n=3/4$  sample is supposed



to contain  $n=3$  and  $n=4$  quantum wells at a ratio of 1:1. The concentration of  $\text{PbI}_2$  is controlled at 0.5M in all samples. Firstly, I made  $n=2$  sample and used it as a tester for the following experiment. 461 mg of  $\text{PbI}_2$ , 201 mg of BAI, and 79 mg of MAI were dissolved in 2 mL of DMF to form a precursor solution of  $n=2$  sample. The precursor solution was completely mixed by a stir bar for 20 minutes. The precursor solution was pre-heated at 70 °C for 20 minutes. The FTO glass substrate was pre-heated at 150 °C for 15 minutes. Then we used a spincoater to fabricate the perovskite film. 150  $\mu\text{L}$  of precursor solution was used to make each sample. The spincoater program was set to 5000 rpm for 20 seconds. The fabricated sample was heated to annealing at 80 °C for 10 seconds immediately after the spincoater process was done. Then we measured the linear absorbance of  $n=2$  sample to check the quantum well population and the light wavelength of the maximum absorption. 461 mg of  $\text{PbI}_2$ , 117.5 mg of BAI, and 112.5 mg of MAI were dissolved in 2 mL of DMF to form a precursor solution of 1:1  $n=3/4$  sample. The sample was fabricated in the same procedure.

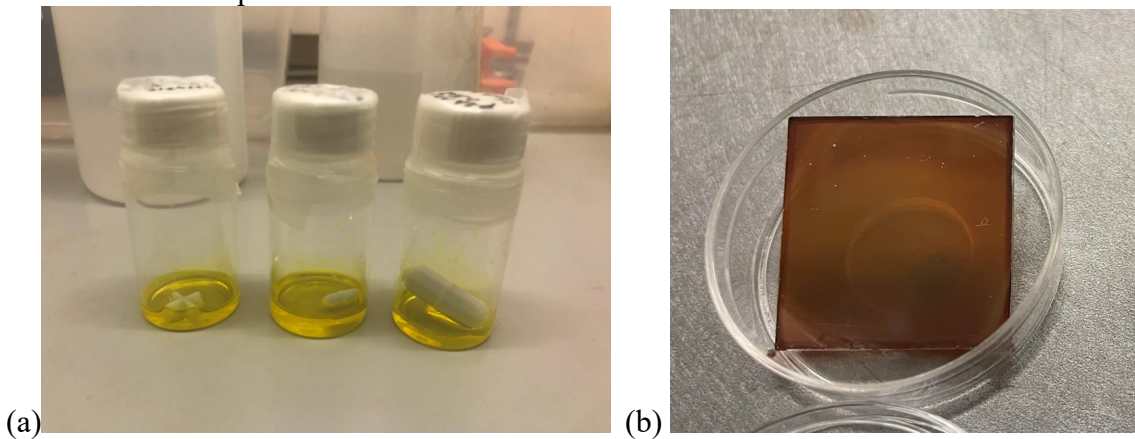


**Figure 8.** These images display a (a) well-mixed precursor solutions and (b) fabricated perovskite layered film sample. A sample contained more large quantum wells will show a darker orange color, while a sample contained more smaller quantum wells will show a lighter orange color.

## 2.2 Nonlinear Fluorescence Spectroscopy

Experiments are conducted with a 45 fs, 4 mJ Coherent Libra with a 1 kHz repetition rate. Continuum pump and probe pulses are generated by focusing 1.5mJ of the 800 nm fundamental beam into a 2m long tube filled with argon gas to induce continuum generation. The generated white light is split by a 70:30 beam splitter as the pump and the probe. The beams are then passed through all-reflective 4F setups, which are based on 1200 g/mm gratings and 20 cm focal length mirrors. Motorized slits (Zaber X-LHM-E Series 100 mm) at the Fourier planes are used to filter the desired portion of the two pulses. The spectrally filtered pulses have 250 fs durations and 5 nm widths. The continuum beams are then relayed into the NLFL setup shown in **Figure 7(a)**. Neutral density filters are utilized to control the pulse energies.

Fluorescence emission from the films is collected using a 5 cm diameter, 5 cm focal length achromatic lens and relayed to 5 cm diameter, 7.5 cm focal length achromatic lens, which focuses the emission onto a photomultiplier tube (PMT, ThorLabs #PMM02). Contributions from scattered light are minimized using an iris and interference filter (Edmund Optics #86-955) that is centered at 725 nm with a 50 nm bandpass. This 50 nm wide bandpass yields sufficient signal-to-noise ratio, while still allowing the laser beams to be tuned to 690 nm. The signal is amplified by applying a 0.7-0.9 V control voltage to the PMT. The fluorescence emission is



measured at 700 nm. The two laser beams are chopped at 500 Hz and 250 Hz, respectively. Thus, signals are acquired under four conditions: pulse 1 only ( $S_1$ ), pulse 2 only ( $S_2$ ), pulses 1 and 2 ( $S_{1+2}$ ), both pulses blocked ( $S_0$ ). The NLFL signal is then defined as following:

$$S_{NLFL} = S_{1+2} - S_1 - S_2 - S_0$$

The signal is averaged over a total of 800 laser shots (0.8 s) at each delay time.

### 3. Results and Discussion:

After fabricating the films using a spincoater, we measured the linear absorbance of the samples first. N=2 sample was used as a tester to figure out the best chemical conditions of sample fabrication. After figuring out the optimized chemical conditions, we used that designed procedure to fabricate n=3/4 sample, which was prepared for the real nonlinear fluorescence scan. N=2 sample was also used to optimize the NLFL setups, such as optimizing the spacial overlapping of the two pulses that were applied to the film. We also used n=2 sample to do several sets of NLFL scans as a test, making sure the whole setup was under a good situation for the following n=3/4 sample scan. The linear absorbance of n=3/4 film was shown below. Though the sample was supposed to contain n=3 and n=4 population at a ratio of 1:1, there's a large n=2 population shown as the peak at 570 nm. N=3 population showed a peak at 600 nm. N=4 population was small and the linear absorbance peak was tiny at 630 nm, which is not obvious enough on the *Figure 9*.

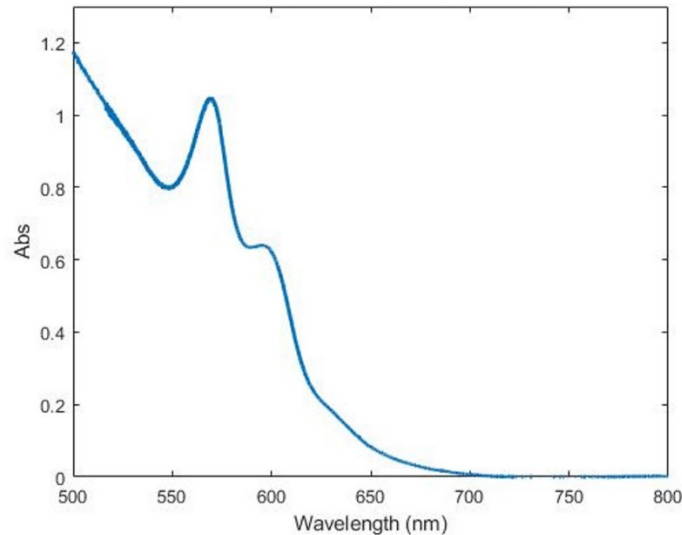


**Figure 9.** The linear absorbance of n=3/4 perovskite film sample. The maximum absorbance peak at 570 nm indicates an n=2 population; The maximum absorbance peak at 600 nm indicates an n=3 population; The maximum absorbance peak at 630 nm indicates an n=4 population.

For the NLFL measurements, we set the pulse 1 at a constant wavelength, while changing the wavelength of pulse 2 over a range from 580 nm to 680 nm. The pulse 1 serves to excite the electrons in the quantum wells and forming excitons. The pulse 2 serves to observe the location of exciton populations after a delay time. The final location of excitons are known by measuring fluorescence at 700 nm, which is the maximum absorbance wavelength of bulk quantum wells.

In this case, we can know the initial location of excitations by setting pulse 1 to a specific wavelength. Then we can know the intermediate location of excitons during their traveling by looking at the wavelength of pulse 2. Finally, through the fluorescence measurement at 700 nm, we know the final location of excitons, which is in those largest quantum wells. The contour figures of NLFL measurements of  $n=3/4$  sample are shown below:

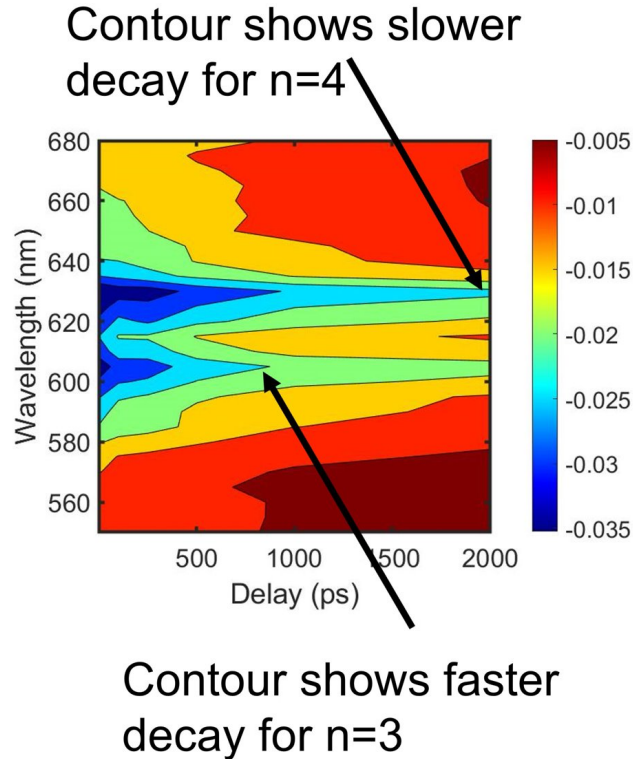


**Figure 10.** The NLFL scan contour graph of  $n=3/4$  sample. The pulse 1 is set at 590 nm. The x-axis is the delay time in pico seconds, and y-axis is the wavelength (nm). The signal intensity is measurement in volts. Blue color indicates a strong signal where exciton population is large. Red color indicates a weak signal where exciton population is small. The blue peak at  $n=600$  nm shows  $n=3$  population, while the blue peak at  $n=630$  nm shows  $n=4$  population.

According to **Figure 10**, as the delay time increases, the signal intensity of  $n=3$  peak decreases faster than the signal intensity of  $n=4$  peak does. For  $n=3$  peak, the blue color disappears when the delay time is about 1000 ps, indicating that the population of excitons in  $n=3$  quantum wells is tiny after 1000 ps. For  $n=4$  peak, the blue color still exists even the delay time reaches 2000 ps, indicating the signal of excitons exists for a longer time than  $n=3$  peak does. As delay time increases,  $n=3$  peak decays faster than  $n=4$  peak does, indicating the energy is transferred from  $n=3$  quantum wells to  $n=4$  quantum wells. By integrating the area under the peak, we have the figure that shows the relationship between population and delay time length, shown as **Figure 10** below. We are integrating the peaks under the assumption of gaussian lineshapes. This makes the numbers less sensitive to noise.

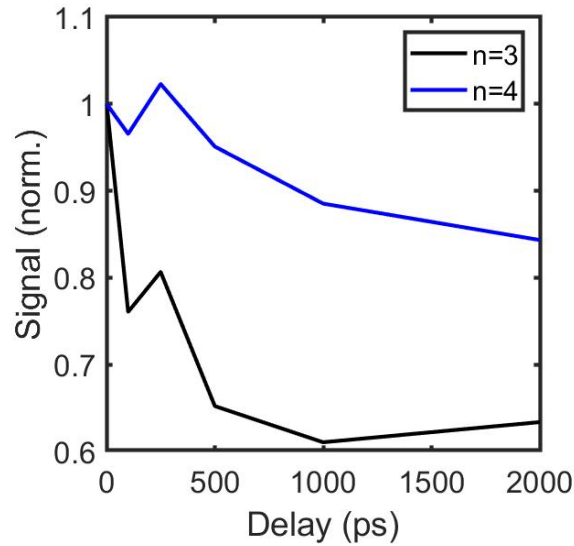


**Figure 10.** Population changes over different delay times. The x-axis represents the delay time in ps, and the y-axis shows the population magnitude. As the delay time increases, n=3 population decreases while n=4 population increases, indicating an energy transfer between n=3 quantum wells and n=4 quantum wells. N=3 quantum well is an energy donor, and n=4 quantum well is an energy acceptor.

The integrated areas are proportional to the number of excitons photoexcited by pulse 1, which is remaining in the film. The n=3 peak decays because those excitons are being converted into n=4 excitons by the energy transfer process. For both n=3 and n=4 signals, there are accident increase of signal intensity as the delay time increases, which are noises. Ideally, the signal intensity will keep decreasing as the delay time increases.

#### 4. Conclusion

In conclusion, by applying nonlinear absorbance spectroscopy on 2D layered perovskite film sample, we see an evidence of energy transfer between n=3 quantum wells and n=4 quantum wells. Generally, energy transfers from smaller quantum wells to larger quantum wells simultaneously, and keep travelling all the way down to the bulk quantum wells. The energy transfer was observed as the change of exciton populations at different delay times. As the delay time increases, the exciton population in n=3 quantum wells decreases faster than that in n=4 quantum wells does, indicating that the energy transfers from n=3 quantum wells to n=4 quantum wells, and continually travel to bigger quantum wells.

## Reference:

1. I. C. Smith, E. T. Hoke, D. Solis-ibarra, M. D. McGehee, and H. I. Karunadasa, *Angew. Chem., Int. Ed.* **53**, 11232–11235 (2014).
2. R. Yang, R. Li, Y. Cao, Y. Wei, Y. Miao, W. L. Tan, X. Jiao, H. Chen, L. Zhang, Q. Chen, H. Zhang, W. Zou, Y. Wang, M. Yang, C. Yi, N. Wang, F. Gao, C. R. 787 McNeill, T. Qin, J. Wang, and W. Huang, *Adv. Mater.* **30**, 1804771 (2018).
3. L. Yan, J. Hu, Z. Guo, H. Chen, M. F. Toney, A. M. Moran, and W. You, *ACS Appl. Mater. Interfaces* **10**, 33187–33197 (2018).
4. J. Zhang, J. Qin, M. Wang, Y. Bai, H. Zou, J. K. Keum, R. Tao, H. Xu, H. Yu, S. Haacke, and B. Hu, *Joule* **3**, 3061–3071 (2019).
5. M. Yuan, L. N. Quan, R. Comin, G. Walters, R. Sabatini, O. Voznyy, S. Hoogland, Y. Zhao, E. M. Beaugregard, P. Kanjanaboos, Z. Lu, D. H. Kim, and E. H. Sargent, *Nat. Nanotechnol.* **11**, 872–877 (2016).
6. H. Zhang, Q. Liao, Y. Wu, Z. Zhang, Q. Gao, P. Liu, M. Li, J. Yao, and H. Fu, *Adv. Mater.* **30**, 1706186 (2018).
7. J. Liu, J. Leng, K. Wu, J. Zhang, and S. Jin, *J. Am. Chem. Soc.* **139**, 1432–1435 (2017).
8. C. C. Stoumpos, D. H. Cao, D. J. Clark, J. Young, J. M. Rondinelli, J. I. Jang, J. T. Hupp, and M. G. Kanatzidis, *Chem. Mater.* **28**, 2852–2867 (2016).
9. O. F. Williams, N. Zhou, J. Hu, Z. Ouyang, A. Kumbhar, W. You, and A. M. Moran, *J. Phys. Chem. A* **123**, 11012–11021 (2019).
10. Smith, I. C., Hoke, E. T., Solis-ibarra, D., McGehee, M. D. & Karunadasa, H. I. A Layered Hybrid Perovskite Solar-Cell Absorber with Enhanced Moisture Stability. *Angew. Chem., Int. Ed.* **53**, 11232-11235 (2014).
11. Yang, R. *et al.* Oriented Quasi-2D Perovskites for High Performance Optoelectronic Devices. *Adv. Mater.* **30**, 1804771 (2018).
12. Ren, H. *et al.* Efficient and Stable Ruddlesden–Popper Perovskite Solar Cell with Tailored Interlayer Molecular Interaction. *Nat. Photonics* **14**, 154-163 (2020).
13. Stoumpos, C. C. *et al.* Ruddlesden–Popper Hybrid Lead Iodide Perovskite 2D Homologous Semiconductors. *Chem. Mater.* **28**, 2852-2867 (2016).